Coarsening dynamics of dewetting nanodroplets on chemically patterned substrates

M. Asgari and A. Moosavi*

Department of Mechanical Engineering, Sharif University of Technology, Azadi Avenue, P.O. Box 11365-9567, Tehran, Iran

(Received 8 April 2012; revised manuscript received 12 June 2012; published 5 July 2012)

Mesoscopic hydrodynamic equations are solved to investigate coarsening dynamics of two interacting nanodroplets on chemically patterned substrates. The effects of different parameters such as the surface chemical pattern, the slip length, the profile of the disjoining pressure, the size of the droplets, and the contact angles on the coarsening are studied. Our results reveal that the presence of a chemical heterogeneity can enhance or weaken the coarsening dynamics depending on the pattern type and positions of the droplets on the substrate. Also increasing the contact angles to values larger than a critical value may qualitatively change the coarsening process, and the profile of the disjoining pressure and the slippage can appreciably modify the coarsening rate.

DOI: 10.1103/PhysRevE.86.016303 PACS number(s): 47.61.−k, 68.15.+e, 68.08.−p, 68.03.−g

I. INTRODUCTION

Thin liquid films on solid substrates have been subject of many investigations as they may be relevant in widespread natural and technological applications such as eye irrigation, biological cell interaction, tertiary oil recovery, coating, lubrication, integrated circuits, and micro- and nanoelectronic devices, to name just a few. It is well known that thin liquid films are not always stable. It is possible to cover a nonwetting surface with a thin layer of a liquid using conventional techniques such as spin coating, dip coating, or spraying. However, through dynamical processes so-called dewetting gradually deforms the layer and ultimately it attains its equilibrium configuration. As this process is very common in industrial applications it has attracted much scientific and technological interest and is studied both experimentally and theoretically for different materials such as polymer [1–8], liquid crystals [9–11], and liquid metals [12].

In the early stages of the dewetting a pattern of isolated droplets is formed [13–15]. The structure and shape of these droplets have been studied and discussed in Refs. [16,17]. The resultant array of droplets is not stable itself and starts to evolve in a long-time-scale process called coarsening. Such coarsening is observed in many physical systems and is generally a type of pattern formation in which the characteristic length scale between features (here the droplets) increases while the total number of features decreases. The dynamics of coarsening is driven by the reduction of the total energy of system. This process is well studied in the context of phase separation of binary alloys described by the Cahn-Hilliard equation [18–20]. In the context of thin liquid films, coarsening leads to fewer and larger droplets and is due to two mechanisms, namely, collapse and collision. The collapse is based on the mass exchange from smaller to larger droplets. The collision relies on the displacement of droplets over the substrate and merging the droplets into a larger droplet.

Recently, the coarsening dynamics of droplets has become the focus of extensive theoretical and numerical investigations. Glasner and Witelski derived a reduced model based on asymptotic methods to predict the rate of coarsening for a large number of droplets [21]. They obtained a set of ordinary equations for mass and position of the droplets representing the long-time coarsening dynamics of droplets. They also determined the regimes where each of the coarsening mechanisms are dominant [22]. It has been proven analytically that there is an upper bound for the coarsening rate in a time-averaged sense [23]. The results obtained in Ref. [21] can be confirmed by this analytic upper bound and also can be compared with some experimental results [24,25]. The role of physical effects, such as gravity and slippage, on the coarsening dynamics has been already discussed [26,27]. It is shown that the coarsening rate for larger droplets decreases in the presence of gravity while the smaller droplets remain mostly unaffected. Increase of the slippage beyond a critical value could change the occurrence of the collapse and the collision mechanisms and direction of droplet migration.

Two dominant physical factors involved in the dynamics of this problem are intermolecular interactions between the thin liquid layer and the solid substrate and the surface tension [28]. The combined effects of all intermolecular interactions, both attractive and repulsive, could be summarized in an intermolecular potential. There is a discussion about a class of physically reasonable choices of intermolecular potential in the literature [17]. In Ref. [21], some necessary properties of potential energy considered for the coarsening problem have been mentioned. Intermolecular interactions play an important role in removing the singularity associated with contact line movement. A moving contact line coupled with a no-slip condition on the liquid-solid interface results in a multivalued velocity field. One way to remove this singularity is to weaken the no-slip boundary condition via a slip condition. Another proposed way is to incorporate the effect of long-range van der Waals forces between the liquid and the solid [29,30].

In the present study we consider two nanodroplets on a flat substrate as depicted in Fig. 1 and investigate the effect of different parameters on the droplet coarsening. For numerical reasons we restrict our study to two-dimensional droplets. Such droplets have been experimentally studied in Ref. [31]. Most of the studies for the coarsening dynamics are based on solving the thin-film-evolution equations in the lubrication approximation by incorporating the disjoining pressure (DJP) [32–35]. Lubrication models use the long-wave approximation, which does not work for the cases with large contact angles. In order to perform a thorough study and consider all ranges of the contact angles we rather apply the boundary

*moosavi@sharif.edu

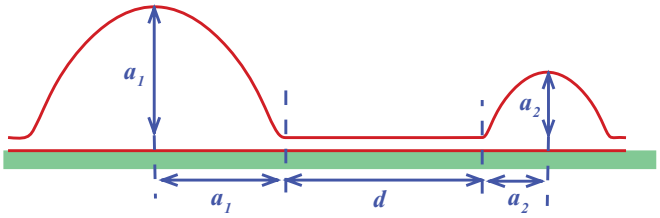

FIG. 1. (Color online) Two droplets placed on a homogeneous surface. The distance between the droplets is d and the sizes of the larger and the smaller droplet are equal to a_1 and a_2, respectively. The initial radius and height of the drops are assumed to be equal to facilitate achieving the equilibrium.

integral method to solve the equations of motion. Very close agreement between the results of this method and those of the lubrication models has been already obtained for small contact angles [36]. Details of the governing equations and a modified version of the boundary integral method that is used in the present study will be discussed in the following section.

II. GOVERNING EQUATIONS AND BOUNDARY CONDITIONS

At the small-Reynolds-number limit, where viscous forces are much larger than inertial forces, the fluid behavior can be simply described by the following equations:

$$\nabla \cdot \mathbf{U} = 0, \tag{1}$$

$$\nabla \cdot \gamma = -\nabla P + \mu \nabla^2 \mathbf{U} = 0, \tag{2}$$

where $\mathbf{U}$ represents the velocity vector and $\gamma_{ij} = -P\delta_{ij} + \mu(U_{i,j} + U_{j,i})$, where P stands for the pressure, δ_{ij} is the Kronecker symbol, and μ denotes the dynamic viscosity of the liquid.

The problem may be converted to a nondimensional form by scaling the lengths with b, which is the equilibrium wetting film thickness, velocity with Ab/μ, where A is a material-dependent parameter, and pressure with σ/b, where σ stands for the surface tension. The dimensionless time is given in units of μ/A [37].

By introducing the stream function ψ ($\partial\psi/\partial y = u_x$, $\partial\psi/\partial x = -u_y$) and vorticity ω ($\omega = \partial u_x/\partial y - \partial u_y/\partial x$) in terms of dimensionless velocity $\mathbf{u}(u_x,u_y)$, the governing equations can be reformulated as [38]

$$\nabla^2 \psi = \omega, \tag{3}$$

$$\nabla^2 \omega = 0, \tag{4}$$

or, equivalently, from the above set of equations, one can show that $\nabla^4 \psi = 0$.

The boundary of the systems under study can be classified into three different groups: those which are in contact with the walls, those which are located at the ends of the system, and those that construct the fluid-vapor interface. For the first type, based on the absence or presence of the slip, we would have no slip ($\psi = 0$ and $\psi_n = 0$) or a slip boundary condition ($\psi = 0$ and $\psi_n = -\beta\psi_{nn}$), respectively, where β represents the slip length. It is worth noting that the contact angle size can affect the slip length [39]. However, in our study we have avoided such complexities and the slip length has been considered constant for all the contact angle ranges. In order to guarantee mass conservation in the system a no-flux boundary condition is considered for the ends. The slope of the interface is also supposed to be zero at the ends of the film. These conditions can be manipulated by setting $\psi = 0$ and $\omega = 0$. At the interface there is no specific value for the unknown variables but the variables can be linked to each other using the fact that the tangential stress on the free surface is zero, i.e., $\sigma_{ij} n_i t_j = 0$, where σ_{ij} is the stress tensor and $\mathbf{t}$ and $\mathbf{n}$ represent the tangential and normal unit vectors along the interface, respectively, and normal stresses $\sigma_{ij} n_i n_j$ are balanced by the DJP and the surface tension. The procedure yields the following:

$$\omega = 2\psi_{ss} - 2\kappa\psi_n, \tag{5}$$

$$\omega_n = -2\psi_{nss} + 2\kappa\psi_{ss} + 2\kappa_s\psi_{ss} - \frac{\kappa_s + \Pi}{\tilde{C}}, \tag{6}$$

where s is the arc length derivative and κ stands for the curvature and may be calculated from

$$\kappa = \frac{y_{ss}x_s - x_{ss}y_s}{\left(x_s^2 + y_s^2\right)^{3/2}}. \tag{7}$$

The parameter $\tilde{C}$ is a scaling factor and the time is scaled with $\mu b/(\tilde{C}\sigma)$ [37]. In order to simplify the comparisons, we simply consider $\tilde{C}$ in Eq. (6) equal to a constant value (3 in this study) for all the substrates considered in the subsequent sections (homogeneous and heterogeneous). Π is the DJP and is defined as the derivative of the intermolecular potential energy. There are many reasonable choices of intermolecular potential and DJP used in the literature [17]. In this work, the chosen DJP has the following form:

$$\Pi(x,y) = C(x)\left(\frac{1}{y^9} \mp \frac{1}{y^3} + \frac{B}{y^4}\right). \tag{8}$$

This profile of the DJP is derived from Lennard-Jones-type pair potentials [37]. The parameter C is a dimensionless amplitude which compares the strength of the effective intermolecular and surface tension forces. For chemical substrates C is a function of x. The parameter B controls the shape of the DJP. Depending on the sign of long-range term (minus or plus) in Eq. (8), the system can exhibit a different dynamics [37]. We refer to these cases as the minus and the plus cases, respectively. The equilibrium contact angle at any location is defined as the following:

$$\cos\theta_{eq} = 1 + \int_{y_0}^{\infty} \Pi(y)\, dy, \tag{9}$$

where y_0 stands for the precursor film thickness [$\Pi(y_0) = 0$] [37].

III. NUMERICAL ALGORITHM

The boundary integral method is a capturing method [40] that has been given attention in the literature. It has been used to study liquid films in fractures [41], spreading of a blob of fluid [42], free surface flow with a moving contact line [43], evolution of droplets on inclined surfaces [44], and motion of nanodroplets over structured substrates [37].

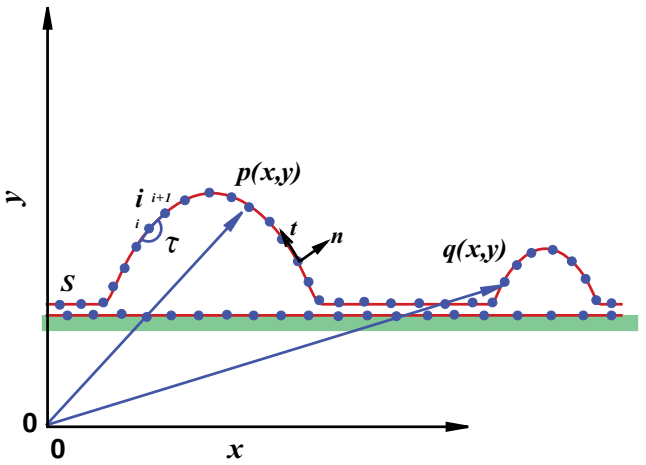

FIG. 2. (Color online) Some explanations about the boundary integral method used for the study. The elements are linear; that is, the nodes are at the ends of the elements and variables change linearly along the element. p can be any point within the system and q can be any point on the boundary S, and θ is the internal angle for boundary points.

Most of the efforts have been performed using constant elements, in which all the variables are assumed to be the same all over the element. Although this representation of the boundary can be considered the simplest possible method of describing the boundary, its characteristics may be useful for avoiding some physical complexities. For instance, it can be used to tackle the singularity that appears at the contact line, the so-called numerical slip technique [43]. A more realistic boundary representation may be obtained by assuming that the nodes are at the ends of the elements and variables change linearly along the element. At any point χ along element i (see Fig. 2) the variables can be obtained in terms of their nodal values through introducing two shape functions. For example, along the element i for variable ψ we have

$$\psi(\chi) = \zeta_i \psi_i + \zeta_{i+1}\psi_{i+1}, \tag{10}$$

where $\zeta_i = \chi$ and $\zeta_{i+1} = 1 - \chi$. The boundary integral method for free surface flow has been described in detail in Ref. [38] but by including linear elements [45] it can be briefly explained as follows: By implementing Green's second identity for the harmonic function ω and a specific function ϕ such that $\nabla^2\phi = \delta(|\vec{p} - \vec{q}|)$, where p can be any point within the system and q can be any point on the boundary S (see Fig. 2), one may write

$$\eta(\vec{p})\omega(\vec{p}) = \int_S [\omega_(\vec{q})\phi_n(\vec{p},\vec{q}) - \omega_n(\vec{q})\phi(\vec{p},\vec{q})]\, ds. \tag{11}$$

Here $\eta(p) = \tau/2\pi$, where τ is the internal angle for boundary points (see Fig. 2) and $\phi = \ln|\vec{p} - \vec{q}|/(2\pi)$. For the case of internal and external points, θ is equal to 1 and 0, respectively. Equivalently, applying the Rayleigh-Green identity for a biharmonic function ψ and a particular function λ, $\nabla^4\lambda = \delta(|\vec{p} - \vec{q}|)$, leads to

$$\eta(\vec{p})\psi(\vec{p}) = \int_S [\psi(\vec{q})\phi_n(\vec{p},\vec{q}) - \psi_n(\vec{q})\phi(\vec{p},\vec{q}) + \omega(\vec{q})\lambda_n(\vec{p},\vec{q}) - \omega_n(\vec{q})\lambda(\vec{p},\vec{q})]\, ds, \tag{12}$$

where $\lambda = |\vec{p} - \vec{q}|^2[\ln|\vec{p} - \vec{q}| - 1]/(8\pi)$. With the help of Eq. (10) and introducing

$$H_{ij} = \frac{1}{2\pi}\left(\int_{S_j} \zeta_j\phi_n(\vec{p},\vec{q})dq + \int_{S_{j-1}} \zeta_{j-1}\phi_n(\vec{p},\vec{q})ds\right) - \eta(p)\delta_{ij}, \tag{13}$$

$$G_{ij} = \frac{1}{2\pi}\left(\int_{S_j} \zeta_j\phi(\vec{p},\vec{q})ds + \int_{S_{j-1}} \zeta_{j-1}\phi(\vec{p},\vec{q})ds\right), \tag{14}$$

$$L_{ij} = \frac{1}{8\pi}\left(\int_{S_j} \zeta_j\lambda_n(\vec{p},\vec{q})ds + \int_{S_{j-1}} \zeta_{j-1}\lambda_n(\vec{p},\vec{q})ds\right), \tag{15}$$

$$K_{ij} = \frac{1}{8\pi}\left(\int_{S_j} \zeta_j\lambda(\vec{p},\vec{q})ds + \int_{S_{j-1}} \zeta_{j-1}\lambda(\vec{p},\vec{q})ds\right), \tag{16}$$

Eqs. (11) and (12) may be represented in the form of a system of algebraic equations:

$$H_{ij}\omega_j + G_{ij}\omega_{n_j} = 0, \tag{17}$$

$$H_{ij}\psi_j + G_{ij}\psi_{n_j} + L_{ij}\omega_j + K_{ij}\omega_{n_j} = 0. \tag{18}$$

Equations (17) and (18) for N considered points provide $2N$ equations and $4N$ unknowns, namely, four variables per point (ω, ω_n, ψ, and ψ_n). Therefore, two of the variables per point should be known or at least should be identified in terms of the remaining variables. By finding ψ and ψ_n along the free surface one can obtain the tangential and normal velocities and from those one can calculate new positions via the Euler approximation

$$\mathbf{r}(t + \Delta t) = \mathbf{r}(t) + \mathbf{u}(t)\Delta t. \tag{19}$$

IV. RESULTS

In order to provide the basic information for the subsequent considerations, we first consider the coarsening of nanodroplets on homogeneous substrates. Then, we extend our study to cases with chemically patterned surfaces in the subsequent sections. In order to reduce the computational efforts, analogous to the previous study [46], we consider the size of the larger droplet to be twice the size of the smaller droplet.

For the initial condition of this dynamics, the droplet shape is specified. To start with a profile reasonably close to the relaxed droplet profile, we consider a parabolic profile that is centered about $x = \overline{x}$ and is smoothly connected to the ultra-thin film (UTF), that is,

$$y(x, t = 0) = y_0 + a\left[1 - \left(\frac{|x - \overline{x}|}{a}\right)^2\right]^{|x-\overline{x}|^m+1}, \tag{20}$$

with the droplet height a in the center being equal to half the base width. The initial dimensions of the droplets were considered to be close to the equilibrium values to remove the initial relaxation effect on the dynamics. Most of our cases are simulated at high contact angles and in this range of angles, droplets with equal radii and heights achieve equilibrium faster [47]. In this study, we choose m, which determines the

smoothness of the transition region from the drop to the UTF, to be 10.

In order to study the dynamics, we obtain the evolution of the mass and position of the droplets during the process. As the simulation is two dimensional, the surface area of the droplets, with the assumption of constant density, is used to measure the mass of the droplets. The position of the droplets is determined by obtaining their center of mass in the lateral direction (x axis). The following equations define the surface area (mass) and the center of mass of the droplets, respectively:

$$M_i = \int_{S_i} dA, \tag{21}$$

$$X_i = \frac{\int_{S_i} X dA}{\int_{S_i} dA}, \tag{22}$$

where M_i and X_i represent the mass and position, respectively, of the smaller ($i = s$) or the larger ($i = l$) droplet and S_i is the surface area occupied by each droplet.

A. Coarsening on homogeneous substrates

In this section we consider two droplets on a flat homogeneous substrate and investigate the effect of different parameters such as the droplet distance, the size of the contact angle, and the shape of the profile of the DJP. This step is constructive before considering the chemically patterned substrates because the previous research efforts on droplet coarsening have involved using lubrication theory, which is valid for small contact angles and it is not clear whether the behavior of the system changes qualitatively at large contact angles. A homogeneous substrate can be viewed as a chemically patterned substrate with constitutive media occupied by the same material. The results will help us to explain the behavior of systems with chemical heterogeneities.

1. Droplet distance

By considering the models derived in Refs. [21,27], it can be concluded that the mass flux between the droplets changes with the distance between the droplets. Close-together droplets exchange mass and evolve faster than droplets that are far from each other. In order to provide further information, two droplets depicted in Fig. 1 are considered with different distances (d). In the case of two droplets, because both of the droplets migrate in the same direction, a collision is not possible and coarsening occurs due to the collapse mechanism. The smaller droplet loses mass at the expense of the larger one growing until it vanishes completely. Figure 3 compares the

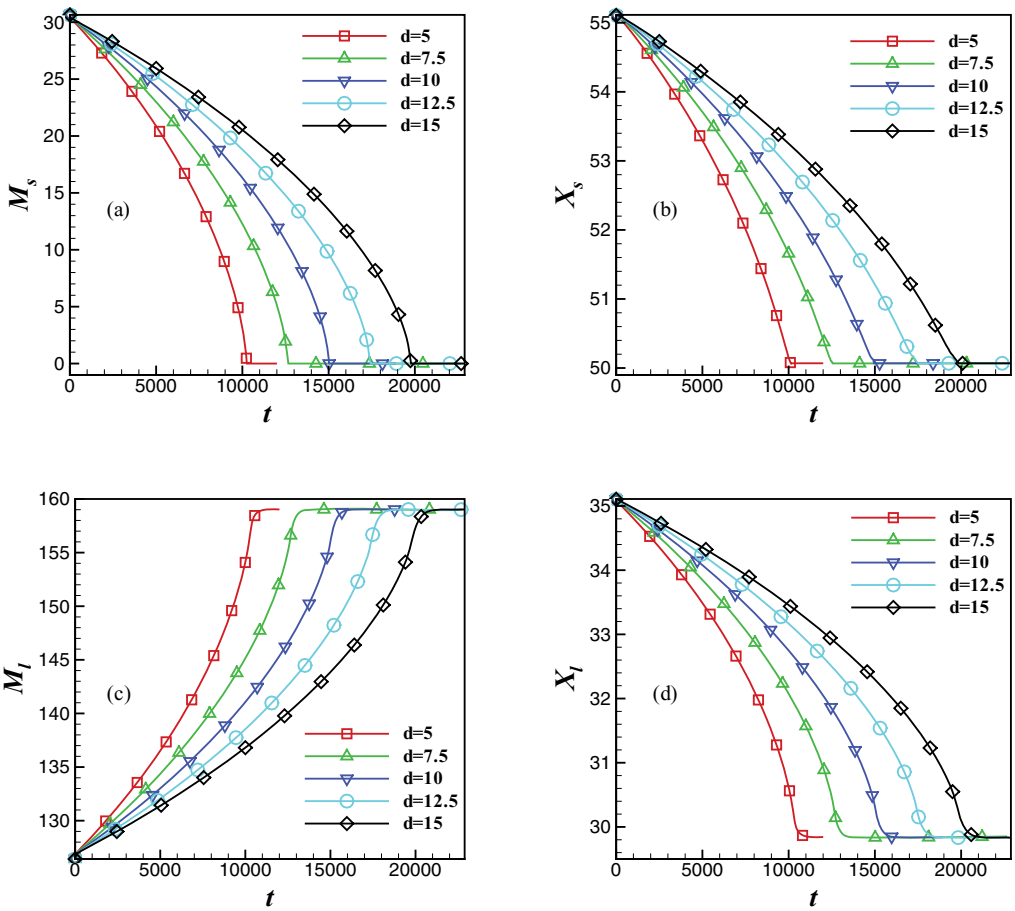

FIG. 3. (Color online) The effect of droplet distance on the coarsening dynamics. Droplets are located on a homogeneous surface with $\theta_{eq} = 120^\circ$. Collapse of the smaller droplet (a), migration of the smaller droplet (b), growth of the larger droplet (c), and migration of the larger droplet (d) are compared for various distances. By increasing the distance, the collapse time increases. For all the considered cases $a_1 = 10$, $a_2 = 5$, and $B = 0$.

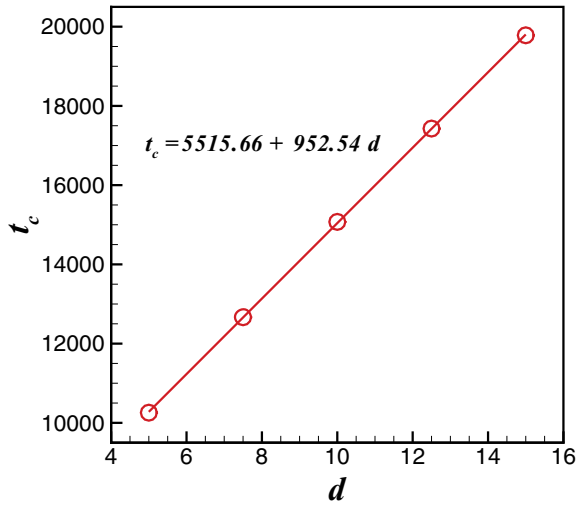

FIG. 4. (Color online) The collapse time vs droplet distance. t_c represents the time required for the smaller droplet to vanish and d is the droplet distance. The small circles are the numerical results and, as can be seen, the coarsening time increases linearly with distance. For all the considered cases $a_1 = 10$, $a_2 = 5$, and $B = 0$.

collapse, growth, and migration of the droplets for different distances. In Fig. 3 and all the following figures M_i and X_i, where the subscript i can refer to the smaller (s) or the larger (l) droplet, represent the mass and position of the center of mass of droplet i, respectively. It takes a longer time for the smaller droplet to vanish completely as the distance increases. This can be explained using the fact that when the droplets are closer, the pressure gradient between them becomes larger. Assuming a constant pressure difference between the two droplets (by fixing their size), we can conclude that the pressure gradient increases when the distance between the droplets decreases. Larger pressure gradients are associated with larger mass fluxes between the droplets and, thus, a faster coarsening process. Figure 4 shows the collapse time t_c as a function of droplet distance d. It is evident from this figure that the time required for the coarsening process is linearly proportional to the distance between the droplets. This is in agreement with theoretical results of Ref. [48] that the flow rate in the films, Q, is proportional to the gradient of the pressure: $Q \propto \Delta P/d$. It should be noted that the results presented here for the distance between droplets is valid when the collapse mechanism of coarsening dominates. The range of distances considered is large enough to prevent the collision of droplets. If the initial distance between the droplets approaches zero, collision is likely to occur and the behavior of the system changes substantially.

2. *The contact angle and the profile of the disjoining pressure*

We considered various contact angles ranging from low (similar to previous studies) to very large contact angles. Interestingly, we found that a transition occurs in the direction of migration of droplets when the contact angle exceeds a critical value. A similar behavior has already been reported for the case of a slip boundary condition [27]. For cases with a contact angle less than the critical value, the droplets migrate in the opposite direction of the mass flux, as was analytically derived in Ref. [46]. However, our results reveal that, when the contact angle is greater than the critical value, the droplets move in the direction of mass flux. This transition is illustrated in Fig. 5. For the system and conditions considered here ($B = 0$ and no-slip condition) the critical contact angle is about $\theta_{eq} = 75.1^\circ$ for which the droplets remain stationary during the coarsening. Figure 6 explains a method to find the overall droplet movement changes for the larger droplet, $\Delta X_l = X_{l2} - X_{l1}$, due to the coarsening versus the contact angle. As can be seen, the larger droplet travels a greater distance as the contact angle increases and the rate is constant. Figure 6 also shows the change of the coarsening time as a function of the contact angle. The time decreases but the behavior is not linear, although the deviation is small.

As mentioned in Sec. II, two adjustable parameters of the DJP, namely, B and C, characterize the wetting properties of the substrate. For a specific θ_{eq} on a flat substrate, one can find a one-parameter family of pairs (B,C). Nanodroplets on substrates with the same contact angle but with various values of (B,C) assume shapes which differ mainly in the vicinity of the three-phase contact line but are similar in the apex

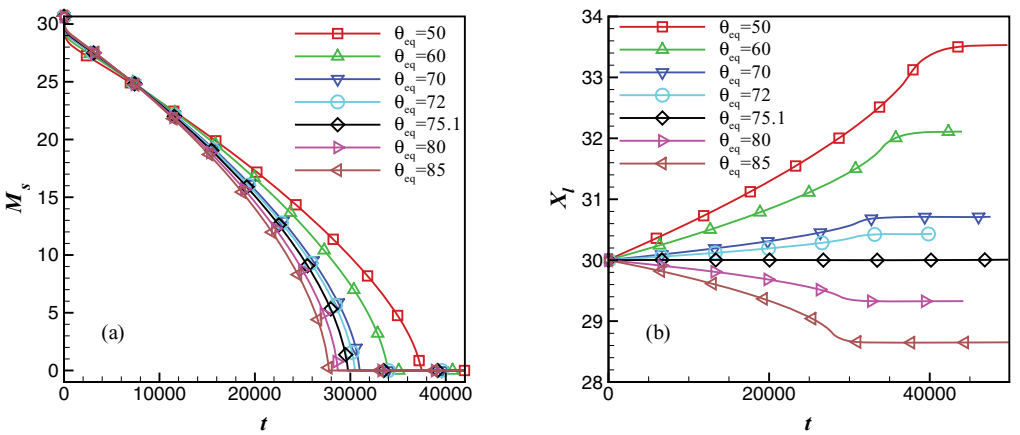

FIG. 5. (Color online) The effect of the contact angle size on the coarsening dynamics. Droplets are located on a homogeneous surface. Collapse of the smaller droplet (a) and migration of the larger droplet (b) are compared for various contact angles. As can be seen, for contact angles larger than $\theta_{eq} = 75.1^\circ$ the direction of migration changes. For all the considered cases $a_1 = 10$, $a_2 = 5$, $d = 5$, and $B = 0$.

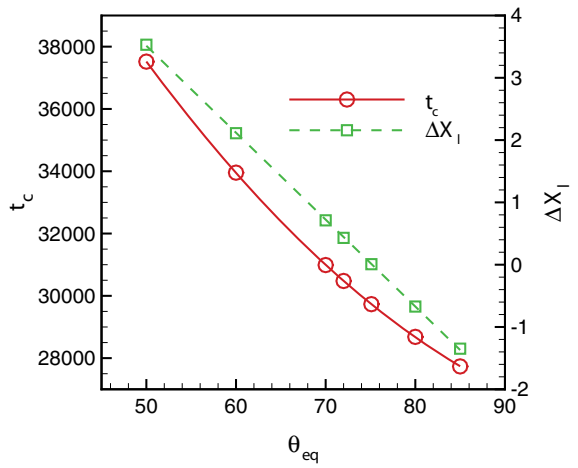

FIG. 6. (Color online) The larger droplet overall migration and smaller drop collapse time vs the surface contact angle. The small circles represent the numerical results. It is seen that there is a change in the migration direction at $\theta_{eq} = 75.1^\circ$. For all the considered cases $a_1 = 10$, $a_2 = 5$, $d = 5$. and $B = 0$.

region [37]. Figure 7 illustrates results for several values of B and C in which the contact angle is kept fixed. (B,C) values for the minus case are $(-1,1.9)$ with $y_0 = 0.88$, $(0,4.0)$ with $y_0 = 1$, and $(1,11.63)$ with $y_0 = 1.3$, and for the plus case the values are $(-2.5,6.38)$ with $y_0 = 0.91$ and $(-4,1.39)$ with $y_0 = 0.79$. The values of B and C are chosen such that in all cases $\theta_{eq} = 120^\circ$. As can be seen the film thickness play an important role in determining the coarsening rate. It is shown that for the same pressure gradients the flow rate through the film is proportional to the cube of the film thickness, $y_f \approx y_0$, i.e., $Q \propto y_f^3$ [48], and this may explain why, for the cases with larger film thickness, coarsening occurs faster. For the minus cases ($B = 0$, 1) the overall coarsening time is less than for the plus cases, which could be related to the film thickness parameter. Also it is seen that the droplets move faster in these minus cases. For the minus case $B = -1$, the film thickness is slightly less than that of the plus case with $B = -2.5$ but the coarsening rate is slightly larger than for the plus case. Although the coarsening rate is larger, the droplets move slower than in the plus case. This indicates that, for the cases with a slight difference in the film thickness, the effect of other parameters such as the form of the DJP profile (see Ref. [37]) should be considered.

B. Coarsening on substrates with chemical heterogeneities

On the nanoscale most surfaces are heterogeneous. These heterogeneities could appreciably change the dynamics of dewetting. There are various recent investigations that have considered the effects of chemical heterogeneities on the early stages of dewetting [49,50]. However, their effects on the final stages of dewetting have not been understood yet. Thus, it is necessary to analyze the coarsening dynamics in the presence of the heterogeneities. In this section, we consider different chemical patterns for the substrates and investigate how they affect the dynamics.

1. Substrates with a favorable chemical gradient

We suppose that there is a wettability gradient in the direction of droplet migration. In other words, the droplets are forced to move in the same direction as the mass flux induced by the coarsening process. This gradient is constructed by changing the contact angle along the solid substrate. Since the direction of migration of the droplets may change by increasing the contact angle, this definition should be carefully considered. The contact angle in a specific position x is given by

$$\theta(x) = \theta_{\max} \mp \alpha(x - x_m), \tag{23}$$

where $\theta_{\max}$ is the maximum contact angle provided at $x = x_m$ and α is the size of the gradient $|\Delta\theta/\Delta x|$. The minus (plus) sign should be considered when the contact angle is smaller (larger) than the critical contact angle. By changing the parameters, we can construct substrates with different gradients. Figure 8(I) represents the results for different gradient sizes. The chosen values for α and $\theta_{\max}$ are such that the contact angle always remains above the critical contact angle and, therefore, the droplets move in the direction of the mass flux. It is evident

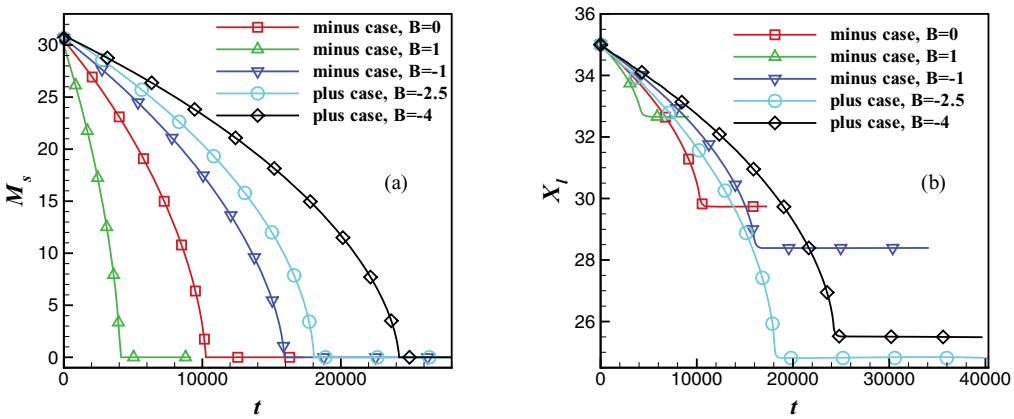

FIG. 7. (Color online) The effect of the disjoining pressure parameters B and C on the coarsening dynamics. Droplets are located on a homogeneous surface. Collapse of the smaller droplet (a) and migration of the larger droplet (b) are compared for various parameters of DJP. The values of B and C are chosen such that in all cases $\theta_{eq} = 120^\circ$. (B,C) values for the minus case are $(-1,1.9)$, $(0,4.0)$, and $(1,11.63)$ and for the plus case they are $(-2.5,6.38)$ and $(-4,1.39)$. For all the considered cases $a_1 = 10$, $a_2 = 5$, and $d = 5$.

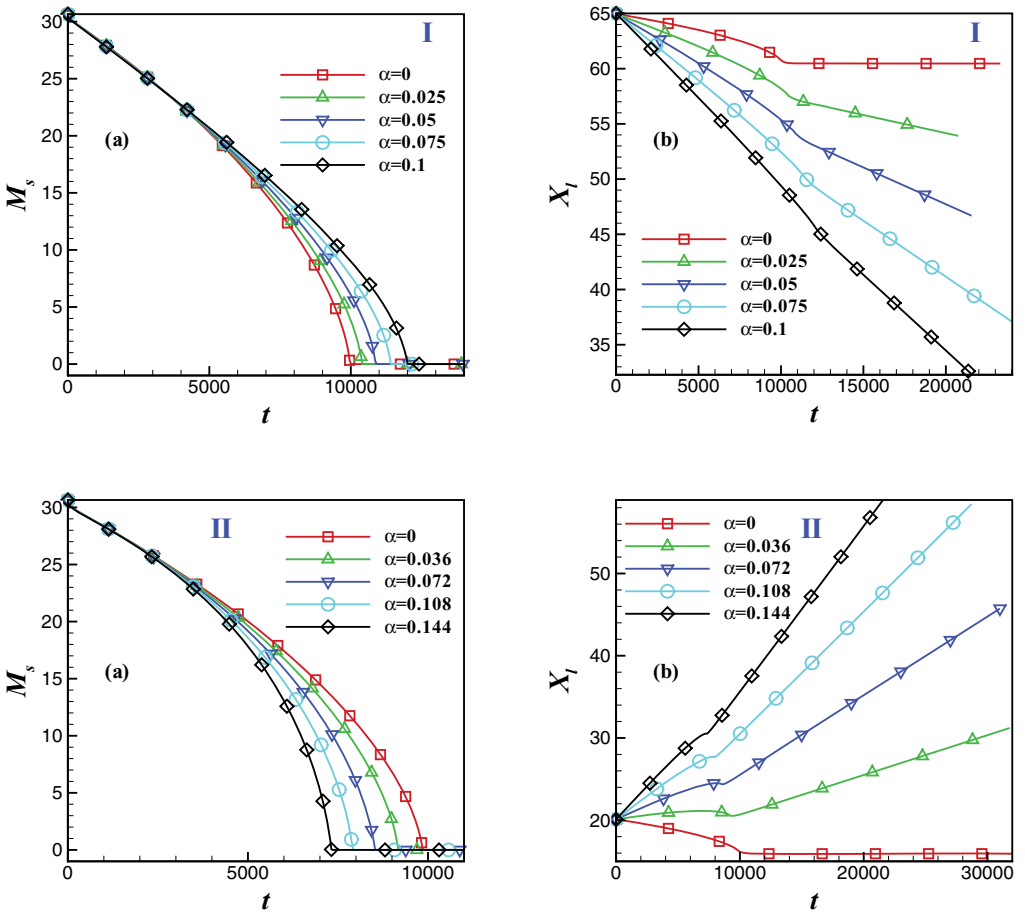

FIG. 8. (Color online) The effect of favorable (I) and unfavorable (II) wettability gradient on the coarsening dynamics. α is the gradient size used to define wettability as $\theta(x) = [110 + \alpha(x - 100)]^\circ$ (I) and $\theta(x) = [110 - \alpha x]^\circ$ (II). Collapse of smaller droplet (a) and migration of larger droplet (b) are compared for various gradient sizes. For all the considered cases $a_1 = 10$, $a_2 = 5$, $d = 5$, and $B = 0$.

that, by increasing the gradient size α, the required time for the coarsening process increases. It is shown that larger droplets have greater velocities on chemical gradient surfaces [36]. Therefore, during the coarsening process, the distance between the droplets increases due to the chemical gradient force and this slows the coarsening process. As is depicted in Fig. 9, in the homogeneous case the distance decreases slightly but for the gradient cases the distance increases with time. Figure 10 depicts the coarsening time as a function of the gradient size. The rate of the increase is not linear and for larger values of α it is greater. This can be explained by considering the results of Ref. [36] for nanodroplets on wettability gradient surfaces for both the small and the large contact angles: that the rate of increase of the velocity is not completely a linear function of the gradient size. For small contact angels, it is shown that the velocity V is proportional to $\theta_O^2\alpha$, where θ_O is the contact angle at the base center of the droplet and, thus, there is a slight deviation from the linear function.

The effect of the slip on the coarsening dynamics has been recently investigated analytically and numerically for small contact angles [27]. A reduced model based on asymptotic methods using the lubrication theory has been derived. Here, we consider a range of slip lengths to explore the effect of this parameter on the collapse and migration rates for droplets

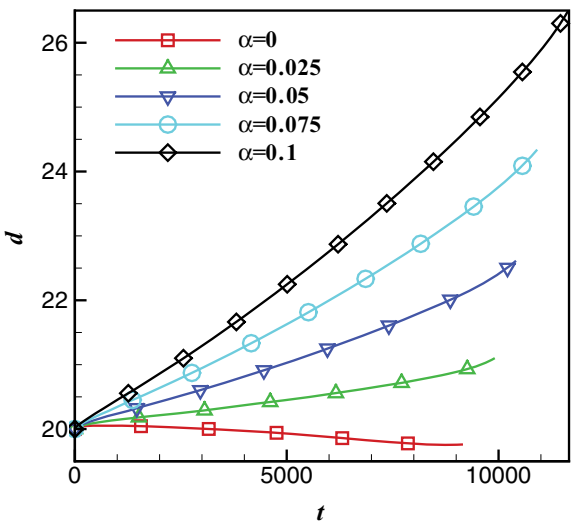

FIG. 9. (Color online) Distance between the droplets during the coarsening process for the favorable gradient case. The results for the homogeneous case has also been included in the figure for comparison purpose. The contact angle is $\theta(x) = [110 + \alpha(x - 100)]^\circ$. For all the considered cases $a_1 = 10$, $a_2 = 5$, $d = 5$, and $B = 0$.

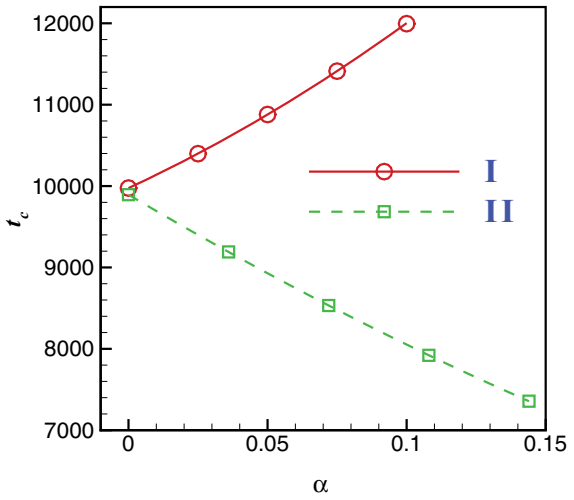

FIG. 10. (Color online) The collapse time vs favorable (I) and unfavorable (II) wettability gradient size along the surface. t_c represents the time required for the smaller droplet to vanish. For all the considered cases $a_1 = 10$, $a_2 = 5$, $d = 5$, and $B = 0$.

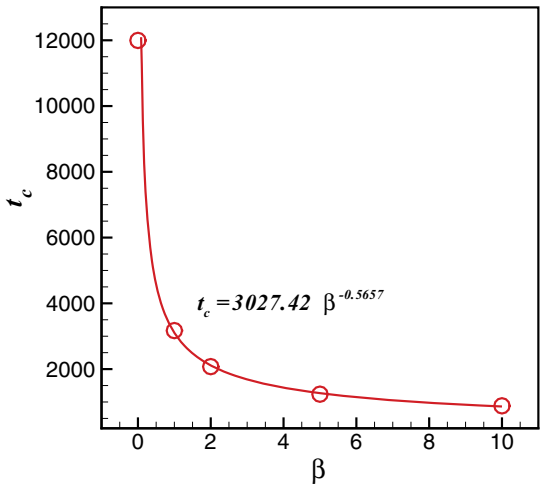

FIG. 12. (Color online) The collapse time as a function of the slip length. t_c represents the time required for smaller droplet to vanish. t_c can be well described in terms of a power-law function of the slip length. The chemical gradient considered along the substrate is $\theta(x) = [110 + 0.1(x - 100)]^\circ$. For all the considered cases $a_1 = 10$, $a_2 = 5$, $d = 5$, and $B = 0$.

positioned on surfaces with a chemical gradient. We only consider cases with a favorable gradient; a similar investigation can be developed for the other case. The contact angle varies as $\theta(x) = [110 + 0.1(x - 100)]^\circ$ along the substrate. Figure 11 shows the results for different slip lengths. By increasing the slip length, the collapse time is reduced while the movement of the droplets increases. These results are in agreement with those of Ref. [27], in which it was concluded that coarsening of droplets is enhanced with a slip boundary condition. In all the cases presented here, the direction of motion of the droplets does not change when the slip length increases. This indicates that the slip length is smaller than the critical value mentioned by Ref. [27]. In order to explain the influence of having a slip boundary condition, Fig. 12 depicts the collapse time versus the slip length. As is evident, the behavior can be well described in terms of a power law of the slip length.

In order to investigate the effect of droplet size (while keeping the size ratio fixed) on the coarsening process, two series of droplets were considered, as depicted in Fig. 13. In the first series the droplets have sizes equal to the cases previously studied, i.e., $a_1 = 10$ and $a_2 = 5$, but in the second series they are larger, i.e., $a_1 = 15$ and $a_2 = 7.5$. Note that scaling the length is done using the thin-film thickness (b), the value of which is different for various systems (typically around 1 nm) [37]. Larger droplets are not modeled because of computational reasons. The interface boundary condition, which includes curvature and disjoining pressure terms, is influenced by the change of the droplet size. The curvature could be defined as the inverse of the spherical drop radius, so changing the drop radius modifies the curvature and also the Laplace pressure. A favorable wettability gradient equal to $\alpha = 0.021$ was also considered along the substrate. Since the distance between the droplets can be defined based on the distance between the center of mass of the droplets [case (I)] or the distance between the adjacent edges of the droplets [case (II)], we considered both cases for the first series. Figure 14

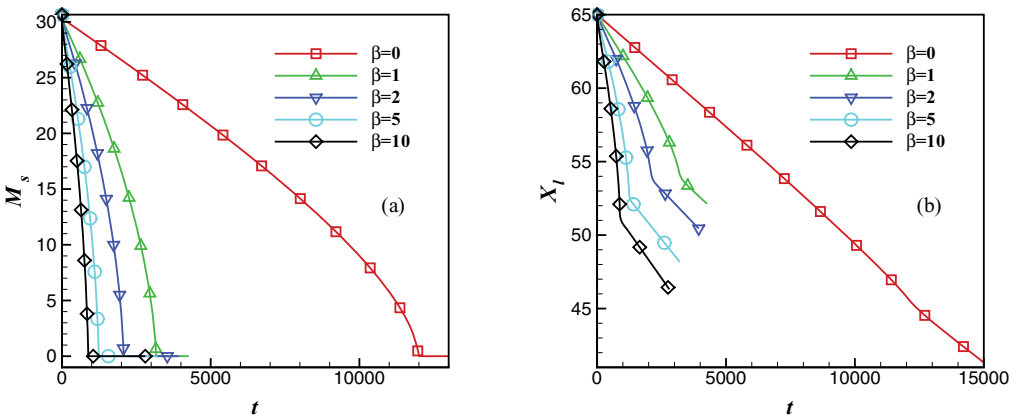

FIG. 11. (Color online) The effect of slip boundary condition on the coarsening. β is the slip length. The chemical gradient considered along the substrate is $\theta(x) = [110 + 0.1(x - 100)]^\circ$. Collapse of the smaller droplet (a) and migration of the larger droplet (b) are compared for a range of slip lengths. For all the considered cases $a_1 = 10$, $a_2 = 5$, $d = 5$, and $B = 0$.

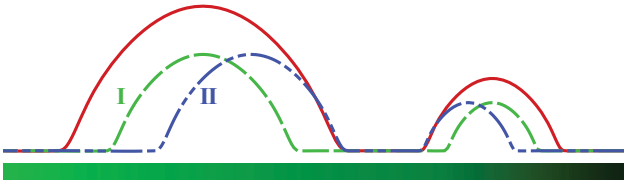

FIG. 13. (Color online) Two series of droplets considered on a substrate with a favorable chemical gradient ($\alpha = 0.021$, $\theta_{\max} = 110^\circ$, and $x_m = 100$) to investigate the effect of droplet size on the coarsening while keeping the size ratio of the droplets fixed. In the first series $a_1 = 10$ and $a_2 = 5$ and in the second series $a_1 = 15$ and $a_2 = 7.5$. For case (I) of the first series the distance between the center of mass of the droplets is equal to that of the second series while for case (II) the distance between the edges, d, is equal to that of the second series.

shows that the velocities of the larger droplets in the second series and those in case (I) of the first series are approximately the same. The gradient size (α) is small and the dynamics is mostly affected by the coarsening process. The coarsening rate is much larger for both cases of the first series. The droplet pressure depends on the size of the droplets ($P_1 \approx \sigma/a_1$ and $P_2 \approx \sigma/a_2$). Since the larger droplet is supposed to be twice the size of the smaller droplet, the pressure difference between the droplets, ΔP, will be $\approx \sigma/2a_2$, which has an inverse relationship with the smaller droplet radius. Thus, by considering a similar or smaller distance between the droplets for the first series, the coarsening time will be smaller because of the larger pressure difference of the first series. The coarsening time for the first series is larger when the distance is calculated based on the distance between the center of mass of the droplets [case (I)]. In this case the pressure gradient is smaller and this weakens the dynamics.

2. *Substrates with an unfavorable chemical gradient*

Unlike the previous part, in this part the chemical gradient is considered in the opposite direction of droplet migration. The contact angle along the substrate is obtained by

$$\theta(x) = \theta_{\max} \pm \alpha(x - x_m). \tag{24}$$

The plus (minus) sign is applied when the contact angle is smaller (larger) than the critical value. By considering the results of the favorable gradient part, it can be expected that an unfavorable gradient enhances the collapse rate. Figure 8(II) illustrates the center of mass of the larger droplet versus time for different wettability gradients. In the absence of a chemical gradient, droplets move in the negative direction along the x axis while the chemical gradient forces the droplets to move in the opposite direction. Therefore, by increasing the gradient size gradually, the direction of motion changes. Nevertheless, for all the gradients considered the coarsening time decreases. Figure 10 also shows the change of the collapse time due to various unfavorable gradient sizes.

3. *Substrates with a chemical stripe*

Chemical heterogeneity of solid substrates can take various forms. One of these forms used in this section is depicted in Fig. 15(I). There is a heterogeneity in the form of a chemical stripe below the larger droplet, which is more wettable than the rest of the surface. Because of this high wettability area, the larger droplet gets pinned over the stripe during the coarsening. We define the contact angle difference as

$$\Phi = \theta_1 - \theta_2, \tag{25}$$

where θ_1 and θ_2 are contact angles of the less and more wettable parts of the substrate, respectively. Figure 16(I) compares the collapse and the migration of the droplets for different values of the contact angle difference. The size of the heterogeneity is supposed to be 14 (smaller than the base width of the larger droplet). The presence of the heterogeneity decreases the distance between the droplets because both droplets start to move initially. However, when the larger droplet arrives at the heterogeneity, it gets pinned and does not move further, but the smaller droplet continues its motion toward the larger droplet and this decreases the distance between the droplets gradually and enhances the dynamics. By decreasing the

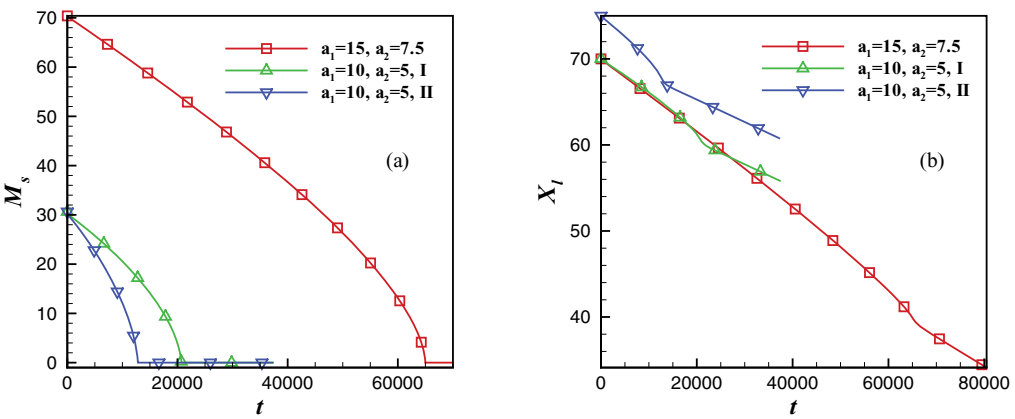

FIG. 14. (Color online) The effect of droplet size on the coarsening rate. Cases (I) and (II) in the figures refer to the first series of droplets ($a_1 = 10$ and $a_2 = 5$). In case (I) the distance between the center of mass of the droplets is the same as that of the larger droplets ($a_1 = 15$ and $a_2 = 7.5$) but in case (II) the droplets have an edge-to-edge distance equal to that of the larger droplets. Collapse of smaller droplet (a) and migration of larger droplet (b) are compared to show the size effect. Increasing the size of the droplets does not change the velocity of the larger droplet during the coarsening. However, the coarsening rate has been decreased considerably. For all the considered cases $B = 0$.

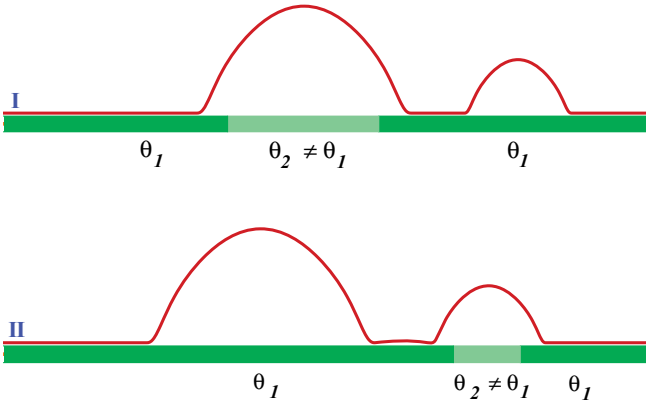

FIG. 15. (Color online) Two droplets placed on a chemical substrate to investigate the effect of this heterogeneity on the coarsening process. In case (I) the heterogeneous part is below the larger droplet and in case (II) the chemical part is below the smaller droplet.

size of the heterogeneity, the distance that the larger droplet can travel increases and the effect of chemical heterogeneity weakens. However, the size of the contact angle difference has little effect on the collapse rate. This fact is depicted in Fig. 17, where the time is reduced with a large slope when the heterogeneity is added to the system but increasing the value of Φ does not change appreciably the collapse time. The collapse time in these cases can be described in terms of a power-law function of Φ. If the stripe is placed below the smaller droplet [see Fig. 15(II)], the collapse and migration rates decrease as depicted in Fig. 16(II). The smaller droplet gets pinned on the stripe area but the larger droplet continues its motion and, as a result, the distance between the droplets gradually increases. Figure 17 also indicates that the collapse time again can be given by a power-law function of Φ for this case.

The chemical stripe can be less wettable than the rest of the substrate, as displayed in Fig. 18. All the contact angles are larger than the critical value. The larger droplet is initially placed on the less wettable part but it gradually moves toward the more wettable part during the coarsening. This increases the distance between the droplets, as shown in Fig. 18(a), and the rate of the coarsening decreases. In contrast, if the smaller droplet is initially considered on the less wettable part, the smaller droplet moves toward the larger droplet and this decreases the coarsening time. If the larger droplet is close to the stripe the droplets may coalesce, which is obvious in

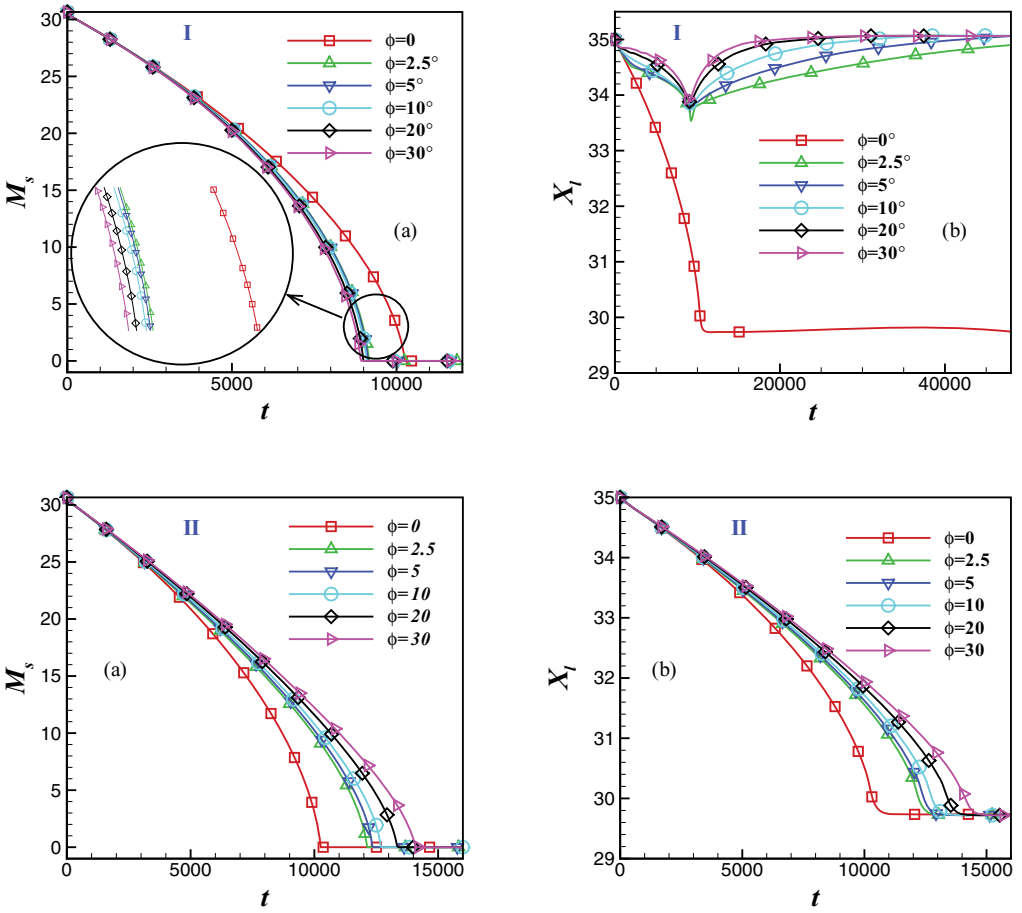

FIG. 16. (Color online) The effect of a more wettable part, which is placed below the larger droplet (upper cases) or the smaller drop (lower cases), on the coarsening dynamics. $\Phi = \theta_1 - \theta_2$ is the contact angle difference between the less (θ_1) and more (θ_2) wettable parts of the substrate. Collapse of the smaller droplet (a) and migration of the larger droplet (b) are compared for various values of the wettability change. For all the considered cases the size of the heterogeneity is equal to 14 for (I) and 6 for (II), which is smaller than the base width of the droplet, and $\theta_1 = 120^\circ$, $a_1 = 10$, $a_2 = 5$, $d = 5$, and $B = 0$.

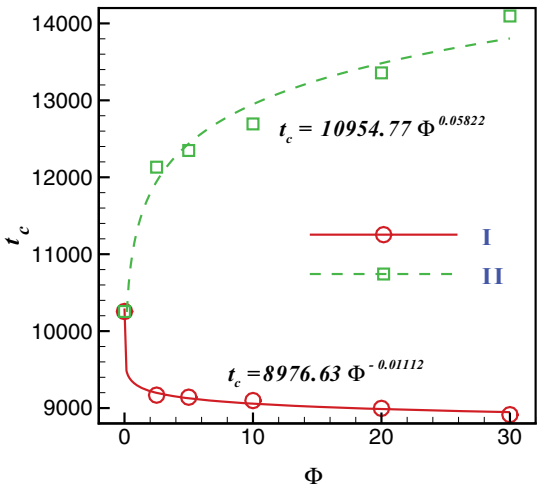

FIG. 17. (Color online) The collapse time vs the contact angle difference $\Phi = \theta_1 - \theta_2$ for the case of a more wettable chemical heterogeneity (I) below the larger droplet and (II) below the smaller droplet. The behavior of the system can be well described by a power-law-type distribution. For all the considered cases the size of the heterogeneity is equal to (I) 14 or (II) 6 and $\theta_1 = 120^\circ$, $a_1 = 10$, $a_2 = 5$, $d = 5$, and $B = 0$.

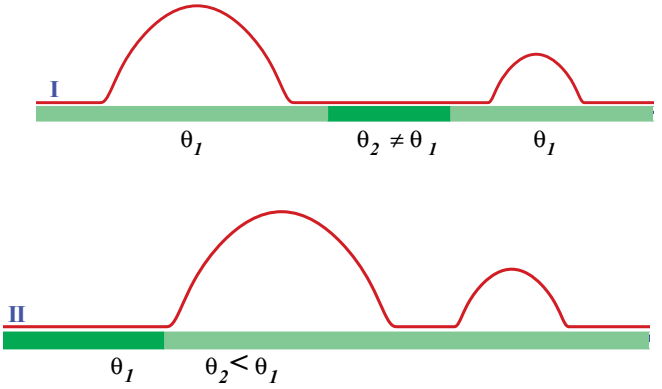

FIG. 19. (Color online) Two droplets placed on a chemical substrate to investigate the effect of the heterogeneity on the coarsening process. In case (I) the heterogeneity is located between two droplets and in (II) the heterogeneity is in the form of a chemical step.

Fig. 18(b). In both cases, it should be noted that the direction of droplet motion is determined by coarsening dynamics, which is in the direction of mass flux for contact angles larger than the critical value.

If both droplets are positioned on the more wettable part and the heterogeneity is located between the two droplets, as shown in Fig. 19, our results indicate that the changes of the collapse and migration of the droplets are negligible as long as the smaller droplet does not arrive at the stripe during the coarsening. If the size of the heterogeneity is large enough, the smaller droplet will reach it and get pinned. Since the larger droplet continues its motion, the distance between the droplets increases and the coarsening rate decreases.

4. *Substrates with a chemical step*

In a different scenario, the droplets are positioned on the more wettable part of a chemical step to study the effect of the step on the coarsening dynamics, as is shown in Fig. 19(II). The contact angles are larger than the critical value and because of the coarsening the droplets start to move toward the step. When the larger droplet arrives at the step it gets pinned and does not move further. This decreases the distance between the droplets continuously and the time of the coarsening decreases. When the larger droplet grows, its center of mass moves away from the step and this further decreases the distance between the droplets and the coarsening time. Figure 20 compares the

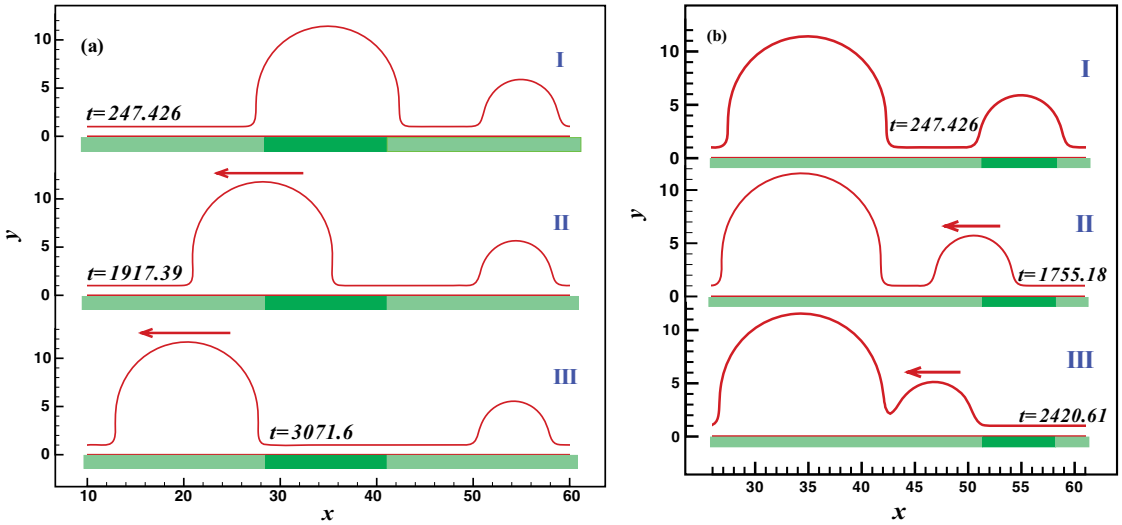

FIG. 18. (Color online) The effect of a less wettable stripe on the coarsening dynamics. The contact angle of the stripe is equal to 130° and the rest parts of the substrate have contact angles equal to 120°. The less wettable stripe is located below (a) the larger drop and (b) the smaller one, respectively. For all the considered cases $a_1 = 10$, $a_2 = 5$, $d = 5$, $B = 0$, and the stripe size is equal to 14 and 6 for the cases (a) and (b), respectively. In the figure the times during the transient evolution of the system are also shown.

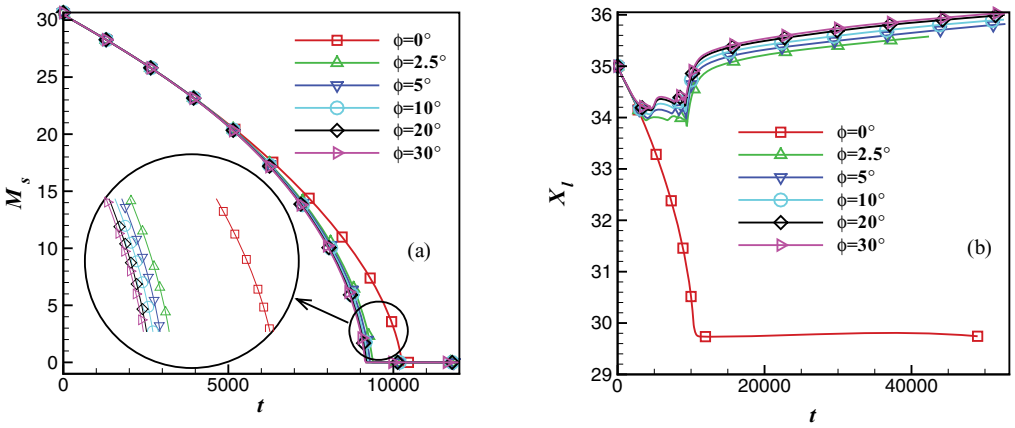

FIG. 20. (Color online) The effect of the chemical step on the coarsening dynamics. $\Phi = \theta_1 - \theta_2$ represents the contact angle difference between the less (θ_1) and more (θ_2) wettable parts of the substrate. Collapse of the smaller droplet (a) and migration of the larger droplet (b) are compared for various values of the wettability change. For all the considered cases $\theta_2 = 120^\circ$, $a_1 = 10$, $a_2 = 5$, $d = 5$, and $B = 0$.

results for various values of $\Phi = \theta_1 - \theta_2$, where θ_1 and θ_2 refer to the contact angles of the less and more wettable parts, respectively. The presence of the heterogeneity reduces the time required for the coarsening process but the size of Φ has no noticeable effect on the time. The rate of decrease of the coarsening time can be described by a power-law function of Φ, as is shown in Fig. 21.

V. CONCLUSION

By using the boundary integral method with linear elements, the coarsening dynamics of two nanodroplets on various types of substrates (homogeneous and chemically patterned) was investigated.

We first considered homogeneous substrates and showed that the dynamics is enhanced linearly when the distance between the droplets decreases. By studying cases with large contact angles, beyond the lubrication approximation, unexpectedly, we found that a transition occurs in the migration direction of the droplets when the contact angle exceeds a critical value. For cases with a contact angle less than the critical value the droplets move in the opposite direction of the mass flux but, when the contact angle is greater than the critical value, the droplets migrate in the direction of the mass flux. Also the coarsening dynamics is enhanced when the contact angle increases. The form of the disjoining pressure was another parameter whose effect on the process was investigated. The type of DJP (plus or minus) could extensively affect the dynamics. Our results revealed that basically the minus case of the DJP reduces the overall time for the coarsening in comparison with the plus case. Although the effect of disjoining pressure is almost explained by the film thickness change, for cases with a slight difference in the film thickness, the form of the DJP could unexpectedly modify the dynamics.

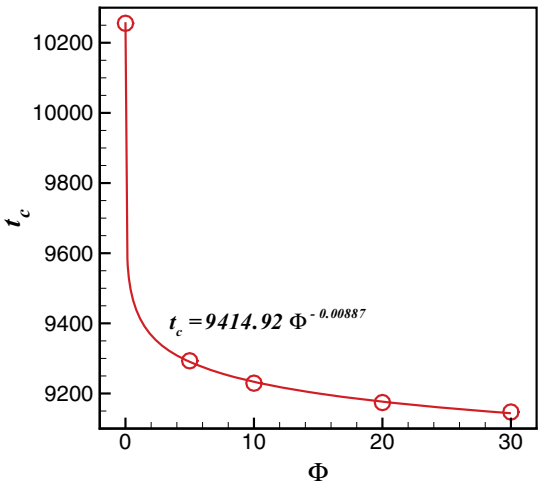

FIG. 21. (Color online) The collapse time vs the contact angle difference $\Phi = \theta_1 - \theta_2$ for a chemical step. t_c represents the time required for the smaller droplet to vanish. The small circles are the numerical results. A power-law distribution is used to model the behavior of the system. For all the considered cases $\theta_2 = 120^\circ$, $a_1 = 10$, $a_2 = 5$, $d = 5$, and $B = 0$.

In this work, different chemically patterned substrates were considered and their effect on the coarsening physics was investigated. By considering droplets on wettability gradient substrates, it was found that if the gradient is in the direction of migration of the droplets (favorable gradient), the dynamics is weakened. The employed gradient is compatible with the droplet migration due to coarsening in this case, though it weakens the dynamics. This fact was explained by analyzing the gradient effect on drop distance during the process. The gradient drives the larger droplet faster in the direction of mass flux and, as a result, the relative mass flux entering the droplet becomes smaller. As the gradient size becomes larger, the dynamics is further weakened. In contrast to the previous case, if the gradient is in the opposite direction of migration of the droplets (unfavorable gradient), the dynamics is enhanced and the coarsening time decreases. It was shown that applying an unfavorable wettability gradient could result in a transition in droplet migration direction. To examine the influence of the slip boundary condition, we considered the favorable gradient case and increased the slip length from zero (no slip) to large values. Increasing the slip length boosts the dynamics and increases the coarsening rate. It was shown that the coarsening time can be well described by a power-law

function of the slip length. We also considered substrates with a chemical stripe. If the stripe is more wettable than the rest of the substrate and considered below the larger (smaller) droplet, the larger droplet (smaller) gets pinned on this part and the smaller (larger) droplet approaches (moves away from) it and, as a result, the pressure gradient between the droplets increases (decreases) and this leads to a faster (slower) coarsening process. Although the existence of a chemical stripe below each of the drops could extensively modify the dynamics as explained, changing the wettability of the stripe does not influence the coarsening process. When the stripe is less wettable than the rest of the substrate, the droplets move away from the stripe region and this enhances (weakens) the dynamics if the stripe is placed below the smaller (larger) droplet. Another remarkable, unexpected point observed in our results is that a chemical stripe located between two droplets does not influence the dynamics at all. We have tried different wettabilities for the stripe but the results are unchanged. Our results also indicated that the presence of a stepwise wettability reduction enhances the dynamics and boosts the coarsening process by making the larger droplet get pinned on its position. Eventually, for cases when the droplets are positioned on the more wettable part of the chemical step, interestingly we found that the existence of a chemical step reduces the coarsening time but the amount of wettability change in the step position does not have any influential effect on the dynamics.

Finally, it could be helpful to indicate some issues that can be considered for further study in the field. Our investigation considers only a two-dimensional analysis. Thus, extending the discussion to three-dimensional systems seems to be a crucial task to understand the physics completely. Also, the systems considered in this study are limited to the interaction of two isolated droplets; however, considering systems with more droplets may possibly reveal new physics. It would be also valuable to address the effects of issues such as evaporation and condensation, viscoelasticity, external body forces, and the Marangoni effect due to temperature and surfactant concentration gradients. The considered heterogeneities in the study are chemical. It would be interesting to study the effects of topographical heterogeneities on the coarsening dynamics. It has been shown that the study of the dynamics on physical heterogeneities can incorporate laterally varying disjoining pressure [37].

[1] P. Volodin and A. Kondyurin, J. Phys. D **41**, 065307 (2008).
[2] G. Reiter, Phys. Rev. Lett. **68**, 75 (1992).
[3] R. Konnur, K. Kargupta, and A. Sharma, Phys. Rev. Lett. **84**, 931 (2000).
[4] A. Sharma and R. Khanna, J. Chem. Phys. **110**, 4929 (1999).
[5] A. Sharma and R. Khanna, Phys. Rev. Lett. **81**, 3463 (1998).
[6] C. Neto, K. Jacobs, R. Seemann, R. Blossey, J. Becker, and G. Grün, J. Phys.: Condens. Matter **15**, 3355 (2003).
[7] R. Xie, A. Karim, J. F. Douglas, C. C. Han, and R. A. Weiss, Phys. Rev. Lett. **81**, 1251 (1998).
[8] G. Reiter, A. Sharma, A. Casoli, M.-O. David, R. Khanna, and P. Auroy, Langmuir **15**, 2551 (1999).
[9] S. Herminghaus, K. Jacobs, K. Mecke, J. Bischof, A. Fery, M. Ibn-Elhaj, and S. Schlagowski, Science **282**, 916 (1998).
[10] F. Vandenbrouck, M. P. Valignat, and A. M. Cazabat, Phys. Rev. Lett. **82**, 2693 (1999).
[11] M. P. Valignat, S. Villette, J. Li, R. Barberi, R. Bartolino, E. Dubois-Violette, and A. M. Cazabat, Phys. Rev. Lett. **77**, 1994 (1996).
[12] J. Bischof, D. Scherer, S. Herminghaus, and P. Leiderer, Phys. Rev. Lett. **77**, 1536 (1996).
[13] F. Brochard-Wyart and C. Redon, Langmuir **8**, 2324 (1992).
[14] R. A. Segalman and P. F. Green, Macromolecules **32**, 801 (1999).
[15] A. Sharma and G. Reiter, J. Colloid Interface Sci. **178**, 383 (1996).
[16] V. S. Mitlin and N. V. Petviashvili, Phys. Lett. A **192**, 323 (1994).
[17] A. L. Bertozzi, G. Grün, and T. P. Witelski, Nonlinearity **14**, 1569 (2001).
[18] J. W. Cahn and J. E. Hilliard, J. Chem. Phys. **28**, 258 (1958).
[19] R. L. Pego, Proc. R. Soc. London, Ser. A **422**, 261 (1989).
[20] A. J. Bray, Adv. Phys. **43**, 357 (1994).
[21] K. B. Glasner and T. P. Witelski, Phys. Rev. E **67**, 016302 (2003).
[22] K. Glasner and T. Witelski, Physica D **209**, 80 (2005).
[23] F. Otto, T. Rump, and D. Slepcev, SIAM J. Math. Anal. **38**, 503 (2006).
[24] R. Limary and P. F. Green, Phys. Rev. E **66**, 021601 (2002).
[25] R. Limary and P. Green, Langmuir **19**, 2419 (2003).
[26] M. B. Gratton and T. P. Witelski, Phys. Rev. E **77**, 016301 (2008).
[27] G. Kitavtsev and B. Wagner, J. Eng. Math. **66**, 271 (2010).
[28] J. N. Israelachvili, *Intermolecular and Surface Forces*, 2nd ed. (Academic, New York, 1992).
[29] A. Bertozzi, Not. Am. Math. Soc. **45**, 689 (1998).
[30] C. Huh and L. Scriven, J. Colloid Interface Sci. **35**, 85 (1971).
[31] T. Ondarcüuhu and M. Veyssié, J. Phys. II **1**, 75 (1991).
[32] L. Brusch, H. Kühne, U. Thiele, and M. Bär, Phys. Rev. E **66**, 011602 (2002).
[33] A. Münch, J. Phys.: Condens. Matter **17**, S309 (2005).
[34] A. Münch, B. A. Wagner, and T. P. Witelski, J. Eng. Math. **53**, 359 (2006).
[35] J. Becker, G. Grün, R. Seemann, H. Mantz, K. Jacobs, K. Mecke, and R. Blossey, Nat. Mater. **2**, 59 (2003).
[36] A. Moosavi and A. Mohammadi, J. Phys.: Condens. Matter **23**, 085004 (2011).
[37] A. Moosavi, M. Rauscher, and S. Dietrich, J. Phys.: Condens. Matter **21**, 464120 (2009).
[38] M. A. Kelmanson, J. Eng. Math. **17**, 329 (1983).
[39] R. S. Voronov, D. V. Papavassiliou, and L. L. Lee, Chem. Phys. Lett. **441**, 273 (2007).
[40] H. Tang, L. Wrobel, and Z. Fan, Comput. Mater. Sci. **29**, 103 (2004).
[41] B. Dindoruk and A. Firoozabadi, Phys. Fluids **6**, 3861 (1994).
[42] S. Betelu, J. Diez, L. Thomas, R. Gratton, and B. Marino, Int. J. Numer. Methods fluids **25**, 1 (1997).
[43] A. Mazouchi, C. Gramlich, and G. Homsy, Phys. Fluids **16**, 1647 (2004).
[44] K. B. Glasner, J. Comput. Phys. **207**, 529 (2005).

[45] C. V. Camp and G. S. Gipson, *Boundary Element Analysis of Nonhomogeneous Biharmonic Phenomena* (Springer-Verlag, Berlin, 1992).

[46] K. Glasner, F. Otto, T. Rump, and D. Slepcev, Eur. J. Appl. Math. **20**, 1 (2009).

[47] A. Moosavi, M. Rauscher, and S. Dietrich, Phys. Rev. Lett. **97**, 236101 (2006).

[48] P.-G. de Gennes, F. Brochard-Wyart, and D. Quere, *Capillarity and Wetting Phenomena: Drops, Bubbles, Pearls, Waves* (Springer-Verlag, Berlin, 2003).

[49] A. Sharma, R. Konnur, and K. Kargupta, Physica A **318**, 262 (2003).

[50] D. Simmons and A. Chauhan, J. Colloid Interface Sci. **295**, 472 (2006).